The Effect of a Concentration-Dependent Viscosity on Particle Transport in a Channel Flow with Porous Walls

James G. Herterich, Ian M. Griffiths, and Dominic Vella
OCCAM, Mathematical Institute, University of Oxford, Radcliffe Observatory Quarter, Oxford OX2 6GG, U.K.

Robert W. Field
Dept. of Engineering Science, University of Oxford, Oxford OX1 3PJ, U.K.

The transport of a dilute suspension of particles through a channel with porous walls, accounting for the concentration dependence of the viscosity, is analyzed. In particular, we study two cases of fluid permeation through the porous channel walls: (1) at a constant flux and (2) dependent on the pressure drop across the wall. We also consider the effect of mixing the suspension first compared with point injection by considering inlet concentration distributions of different widths. We find that a pessimal inlet distribution width exists that maximizes the required hydrodynamic pressure for a constant fluid influx. The effect of an external hydrodynamic pressure, to compensate for the reduced transmembrane pressure difference due to osmotic pressure, is investigated. © 2014 American Institute of Chemical Engineers AIChE J, 60: 1891–1904, 2014
Keywords: porous walls, concentration-dependent viscosity, water filtration, concentration polarization

Introduction

Water filtration is becoming increasingly important as a method of water treatment in our everyday lives. Many of the processes are not fully understood, including the crossflow filtration system we consider. A crossflow filtration system consists of a fluid with contaminants (often particulates) flowing tangentially to a porous membrane. This membrane allows the fluid to pass through but rejects the particulates. The filtration is driven by two pressure differences: (1) the hydrodynamic pressure difference across the membrane and (2) the difference in osmotic pressure across the membrane. The osmotic pressure on the filtrate side is generally close to zero, whereas that on the feed side is greater than that in the bulk flow due to the build-up of particles near the membrane surface. This phenomenon is referred to as concentration polarization and is one of the main limitations of the efficacy of water filtration[1] as the high osmotic pressure on the feed side of the membrane reduces the effective pressure that drives filtration.

The fluid velocity in a channel with porous walls has been analyzed for a constant viscosity and constant permeation velocity.[2] The solution is a Poiseuille-like parabolic profile decreasing in magnitude along the channel for the axial component and a transverse component with a cubic dependence on cross-channel position that is proportional to the permeation flux. More generally, with any flow through the porous walls, the axial flow rate in the channel is reduced and, when combined with advection by the transverse flow, results in concentration polarization.[3]

A complicating factor in water filtration using membranes is the dependence of the liquid viscosity on particle concentration. The liquid viscosity is often taken as a constant in models of filtration, but in practice depends on many local properties of the fluid such as its temperature, density, and shear rate. Of particular concern in this article is the effect of concentration-dependent viscosities on crossflow filtration. Davis and Sherwood[4] consider the convection–diffusion equation for particles in a steady-state boundary layer with a concentration-dependent viscosity and diffusivity given by Davis and Leighton.[5] This model assumes that, outside the boundary layer, the bulk concentration of particles is constant. Physically, this may be achieved in a system in which the Péclet number is large so that advection dominates diffusion. A similarity solution in the boundary layer is obtained in this case. Bowen and Williams[6] consider a full numerical solution to the continuity, Navier–Stokes and convective–diffusion equations for crossflow ultrafiltration for concentration-dependent viscosity and diffusion coefficient using a Thomas algorithm. Their results show the significant effect various parameters have on concentration polarization and the rate of filtration.

The transition from concentration polarization to deposition (fouling) on the membrane is of great importance to the lifetime of membranes. Bacchin et. al.[7] model this by a toggle that changes the equations for the permeate flux and wall concentration depending on which is taking place. This toggle is implemented via a critical concentration: below this critical value, concentration polarization occurs, but once above it, there is sufficiently high concentration for particle deposition to occur as well as concentration polarization

Correspondence concerning this article should be addressed to I. M. Griffiths at ian.griffiths@maths.ox.ac.uk.

(i.e., there is some irreversible solidification as a gel or cake formation). The type of driving phenomena may alter the outcome and the critical flux for the transition between concentration polarization and deposition is linked to the local Péclet number.

In this article, we consider a pressure-driven fluid flow with advection and diffusion of particles in a thin porous channel, with aspect ratio $\delta \ll 1$. We study the particular case of a dilute suspension of identical and neutrally buoyant particles and consider a bulk concentration with a specified cross-stream distribution entering the channel. As such, we assume that no deposition of particles on the membrane occurs. Determining the critical concentration, defined in Bacchin et al.,[7] is beyond the scope of this work; rather, our aim is to understand the early stages of particle build-up that ultimately leads to concentration polarization.

We assume that the flow is steady (i.e., constant in time) and examine its variations in space arising due to the local particle concentration and permeation flux through the channel walls. The fluid (but not particles) may pass through the porous walls so that the walls act as perfect filters, and we do not consider the possibility that particles may block pores when they reach the walls. The effects of a concentration dependence of the viscosity of the fluid are analyzed, however, a constant diffusion coefficient is shown to be asymptotically appropriate for a dilute suspension. The form of the channel fluid flow as in Probstein[2] is retrieved as a leading-order solution that does not have a particle concentration dependence, and the higher-order concentration-dependent solution is determined. The case of a pressure-dependent permeation flux is considered, where the hydrodynamic and osmotic pressures drive the filtration. We are particularly interested in the pressures required for a constant inlet fluid flux due to the concentration-dependent viscosity.

We provide a mathematical description of the problem, applying a thin-channel approximation to the governing equations to derive a coupled system of nonlinear partial differential equations. These equations are simplified by examining the asymptotic limit of a dilute suspension of particles and solved with analytic results at leading order and numerical results at the next order. We also consider the effects of an outer pressure, that is, a pressure outside the channel that affects the transmembrane pressure difference. Order-one Péclet numbers are taken so that the advection and diffusion of particles in the channel are equally important, to provide the greatest generality for the particle dynamics in the channel.

Modeling

We consider a two-dimensional channel of length L, with porous walls located at $y = \pm H/2$, as depicted in Figure 1. Fluid is injected into the channel at $x = 0$ at a fixed flow rate, Q (m^2/s), and with a given concentration distribution of particles. The velocity field within the fluid is $\boldsymbol{u} = (u, v)$, with u the axial component and v the transverse component. In such a configuration the solvent (particle-free) viscosity, μ_0, will play a key role in determining the flow profile.

For typical set-ups of interest, we consider channels of length, L, of around a meter (m) and width, H, of order millimeters (mm) so that the channel is thin, with aspect ratio $\delta = 10^{-3}$, flow speeds, $U = Q/H$, of order millimeters per second (mm/s), and particles of typical size, a, of tens of nanometers. Such a parameter regime is applicable to
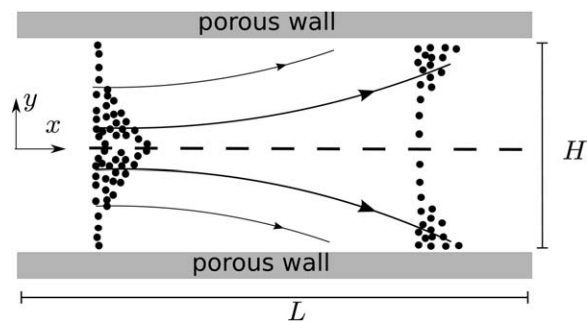
Figure 1. Schematic of a channel with porous walls.

The channel has length L and width H. The fluid flows from left to right and is allowed to leak out through the channel walls. Particles entrained in the fluid with some distribution at the inlet are advected by the flow and diffuse by Brownian motion, collecting at the channel walls.

direct-flow configurations[8] (which are the basis for many designs in the water industry) and may also be applicable to some crossflow scenarios. The density and viscosity of water are $\rho = 1000$ kg/m^3 and $\mu_0 = 10^{-3}$ Pa s, respectively, and $k_B T = 4 \times 10^{-21}$ J at room temperature $T = 300$ K (with Boltzmann's constant k_B). In a thin channel, the ratio of inertial to viscous forces is given by the reduced Reynolds number, $Re = \delta^2 \rho U L / \mu_0 \ll 1$, which is small so that inertial forces may be neglected. The small aspect ratio and Reynolds number offer mathematical simplifications to the analysis. The particles, of size a, are in principle subject to Brownian diffusion ($D_0 = k_B T / 6 \pi \mu_0 a$)[1] and shear-induced diffusion ($a^2 \dot{\gamma}$,[9] for shear rate $\dot{\gamma} = U/H$). However, for $a \approx 10$ nm, Brownian diffusivity dominates. This also gives an order-one reduced Péclet number, $Pe = \delta^2 U L / D_0 = \mathcal{O}(1)$, as D_0 depends on the size of the particle. An $\mathcal{O}(1)$ Péclet number allows for the richest interplay between diffusion and advection.

The particles in the channel are described by their volume fraction, $\phi(x, y)$. The volume fraction of particles at the inlet, $x = 0$, is prescribed by $\phi(x=0, y) = \Phi(y)$ for some function Φ. We wish to understand how the volume fraction, $\phi(x, y)$, changes with distance along the channel as a result of the fluid flow, and how it influences the flow. The viscosity of the fluid, μ, is assumed to be dependent on the volume fraction, writing $\mu = \mu(\phi)$, the functional form of which will be prescribed in due course.

Governing equations

Assuming a small Reynolds number, the fluid flow is governed by the steady Stokes equations, representing conservation of mass and momentum of the fluid

$$\nabla \cdot \boldsymbol{u} = 0 \tag{1a}$$

$$\nabla \cdot \left(\mu(\phi) \left[\nabla \boldsymbol{u} + (\nabla \boldsymbol{u})^T \right] \right) = \nabla p \tag{1b}$$

where p is the hydrodynamic fluid pressure.

The flow advects the particles down the channel, but they also diffuse within the channel. The particle volume fraction is, therefore, governed by the steady advection–diffusion equation

$$\boldsymbol{u} \cdot \nabla \phi = \nabla \cdot (D(\phi) \nabla \phi) \tag{2}$$

Here, $D(\phi)$ is the particle diffusivity, which will in general also depend on volume fraction.

Boundary conditions

Let us now consider the boundary conditions to which the governing equations, (1) and (2), are subjected. The flow and particle distribution are assumed to be symmetric about the axis of the channel, that is

$$\frac{\partial \phi}{\partial y} = \frac{\partial u}{\partial y} = v = 0 \quad \text{on } y=0 \tag{3}$$

Henceforth, we shall consider only the behavior in the half channel $0 \leq y \leq H/2$. We consider the two permeation fluxes through the porous channel walls, $\mathcal{V} := v(x, H/2)$, that are most often found in practical applications. First the case when $\mathcal{V}$ is a constant, say $\mathcal{V}^*$, is considered. In the absence of significant osmotic effects, this type of permeation flux has been achieved by having a flow of fluid (recirculated filtered fluid) outside the channel so that the pressure difference across the membrane is constant along the wall.[10] Second, we consider the case where $\mathcal{V}$ is proportional to the net driving force (i.e., the transmembrane pressure less the difference in osmotic pressure). At the wall, we, therefore, have one of the two possible boundary conditions for the transverse velocity

$$v(x, H/2) = \mathcal{V} = \begin{cases} \mathcal{V}^* = \text{constant} & \text{(Case 1)} \\ \kappa(\Delta p - \Delta \pi) & \text{(Case 2)} \end{cases} \tag{4}$$

respectively, where κ is a constant of proportionality that is related to the solvent viscosity and the permeability of the porous wall and its thickness (cf. Darcy's law). Here, the term $\Delta p = p(x) - p_{\text{outer}}$ is the hydrodynamic pressure difference across the membrane, which is measured relative to the pressure outside the channel, p_{outer} (i.e., the reference pressure). Similarly, $\Delta \pi = \pi - \pi_{\text{outer}}$ where π is the osmotic pressure due to particles in the channel and π_{outer} is that due to particles outside the channel. Here, $\pi_{\text{outer}} = 0$ as we assume complete rejection of particles at the channel wall. The osmotic pressure difference across the porous wall is, in general, a function of the volume fraction of particles at the surface of the porous wall.

In general, at a porous wall there is a tangential slip velocity, whose magnitude is determined by a Neumann boundary condition such as that given by Beavers and Joseph.[11] However, it has been found that this slip is not significant for a wide range of membranes,[12] and so here, for simplicity, we shall assume a no-slip boundary condition

$$u(x, H/2) = 0 \tag{5}$$

as also adopted by Bowen and Williams.[6]

As particles are rejected by the membrane but fluid may permeate, a no-flux boundary condition for the particles at the channel walls is applied. This may be written as[4,7]

$$v\phi - D\frac{\partial \phi}{\partial y} = 0 \quad \text{on } y = H/2 \tag{6}$$

Two final conditions close the system. At the inlet, we impose a constant flow, Q

$$Q = \int_{-H/2}^{H/2} u \, dy = 2 \int_{0}^{H/2} u \, dy \quad \text{at} \quad x=0 \tag{7}$$

At the outlet, the pressure is assumed to be constant; without loss of generality we may set this outlet pressure to zero, that is

$$p = 0 \quad \text{at } x = L \tag{8}$$

but note that this may differ from the pressure outside the channel, ie. p_{outer} may not necessarily be zero. We note that the appropriate outlet boundary condition for a direct-flow configuration is $u=0$ at $x=L$. However, we could in principle choose the outlet pressure such that there is no net outflow. Although these conditions are not identical, the overall behavior in both cases will be similar, except in a small region near the outlet.

Thin-channel approximation

We suppose that the channel is thin so that the aspect ratio $H/L = \delta \ll 1$. We exploit the smallness of δ, nondimensionalizing the system by letting

$$x = L\hat{x}, \quad y = \delta L \hat{y}, \quad u = \frac{Q}{H}\hat{u},$$
$$v = \delta \frac{Q}{H}\hat{v}, \quad \mu = \mu_0 \hat{\mu}, \quad p = \frac{Q\mu_0}{\delta^2 HL}\hat{p}, \tag{9}$$
$$\kappa = \frac{\delta^3 L}{\mu_0}\hat{\kappa}, \quad \pi = \frac{Q\mu_0}{\delta^2 HL}\hat{\pi}, \quad D = D_0\hat{D}$$

in which the dimensionless variables appear with a hat, and μ_0 is the viscosity of the solvent in the absence of particles and D_0 is the constant Brownian diffusion coefficient for a particle in the absence of the effects of surrounding particles. Conservation of mass motivates the transverse velocity scaling being chosen to be the same as the axial velocity scaling multiplied by a factor of δ. However, note that the total fluid permeate may be order unity (despite the small velocity at each point) because of the length of the pipe. Substituting the nondimensionalization (9) into Eqs. 1 and 2 and retaining only leading-order terms in δ provides the equations for the volume fraction in a thin-channel flow with a concentration-dependent viscosity (dropping the hats for convenience)

$$\frac{\partial u}{\partial x} + \frac{\partial v}{\partial y} = 0 \tag{10a}$$

$$\frac{\partial}{\partial y}\left(\mu(\phi)\frac{\partial u}{\partial y}\right) = \frac{\partial p}{\partial x} \tag{10b}$$

$$0 = \frac{\partial p}{\partial y} \tag{10c}$$

$$Pe\left(u\frac{\partial \phi}{\partial x} + v\frac{\partial \phi}{\partial y}\right) = \frac{\partial}{\partial y}\left(D(\phi)\frac{\partial \phi}{\partial y}\right) \tag{10d}$$

Here, Pe is the (reduced) Péclet number

$$Pe = \delta^2 \frac{UL}{D_0} = \delta\frac{Q}{D_0} \tag{11}$$

The Péclet number measures the rate of advection of particles down the channel compared with the diffusion across the channel. As discussed earlier, the viscosity $\mu(\phi)$ is assumed to be a known function. We note that (10c) implies that the hydrodynamic pressure is, to leading order, a function of x only, that is, $p = p(x)$. Note also that Eq. 10d indicates that there is no axial particle diffusion present at leading order in δ.

The dimensionless boundary conditions, to leading order in δ, to be used in determining the solution to (10) are as follows (again dropping hats for convenience)

$$\frac{\partial \phi}{\partial y} = \frac{\partial u}{\partial y} = v = 0 \quad \text{on } y=0 \tag{12a}$$

$$v(x,1) = \mathcal{V} = \begin{cases} \mathcal{V}^* & \text{(Case 1)} \\ \kappa[p - p_{\text{outer}} - \Delta\pi] & \text{(Case 2)} \end{cases} \tag{12b}$$

$$u(x,1) = 0 \tag{12c}$$

$$Pe\, v\phi - \frac{\partial \phi}{\partial y} = 0 \quad \text{on } y=1 \tag{12d}$$

$$\int_0^1 u\, dy = 1 \quad \text{at } x=0 \tag{12e}$$

$$p = 0 \quad \text{at } x=1 \tag{12f}$$

The two cases in Eq. 12b refer to the two distinct permeation fluxes as described in (4): constant, $\mathcal{V}^*$, and pressure-dependent, and will be treated separately. Finally, we specify the volume fraction profile at the inlet

$$\phi(0,y) = \Phi(y) \tag{13}$$

for some $\Phi(y)$. Two natural types of injection that should be compared are (1) uniform injection across $0 \leq y \leq 1$ and (2) point injection. To capture both of these, we consider a normalized particle distribution at the inlet that is Gaussian in nature, of the form

$$\phi(0,y) = \Phi(y) = \frac{\exp\left(\frac{-y^2}{2\sigma^2}\right)}{\sqrt{\frac{\pi}{2}}\, \sigma\, \text{erf}\left(\frac{1}{\sqrt{2}\sigma}\right)} \tag{14}$$

Here, σ is a constant that reflects the width of the distribution. The uniform inlet volume fraction arises in the limit $\sigma \to \infty$, whilst point injection at the center $y=0$ corresponds to $\sigma \to 0$; intermediate values of σ give different pulse widths.

Equations 10 subject to boundary conditions Eq. 12 and inlet condition Eq. 13 define our problem mathematically.

Model solution

Our aim is to determine the change in particle volume fraction, ϕ, as we move down the channel, that is, the variation with y of $\phi(x,y)$ as x increases. Integrating the momentum Eq. 10b, and making use of the symmetry and no-slip conditions (12a, 12c) gives

$$u(x,y) = -\frac{dp}{dx} \int_y^1 \frac{\tilde{y}}{\mu(\phi(x,\tilde{y}))} d\tilde{y} \tag{15}$$

Substituting (15) into the continuity equation, (10a) integrating and applying (12a) gives

$$v(x,y) = \frac{\partial}{\partial x} \left\{ \frac{dp}{dx} \left(y \int_y^1 \frac{\tilde{y}}{\mu(\phi(x,\tilde{y}))} d\tilde{y} + \int_0^y \frac{\tilde{y}^2}{\mu(\phi(x,\tilde{y}))} d\tilde{y} \right) \right\} \tag{16}$$

The transverse fluid velocity at the channel wall, $\mathcal{V}$, is then given by

$$v(x,1) = \mathcal{V} = \frac{\partial}{\partial x} \left\{ \frac{dp}{dx} \left(\int_0^1 \frac{\tilde{y}^2}{\mu(\phi(x,\tilde{y}))} d\tilde{y} \right) \right\} \tag{17}$$

Treating $\mathcal{V}$ as given by the two behaviors of the permeation flux of interest in Eq. 12b, and expanding the derivative in Eq. 17 results in an ordinary differential equation (ODE) for the hydrodynamic pressure, $p(x)$, of the form

$$\frac{d^2p}{dx^2} - \frac{B(x)}{A(x)} \frac{dp}{dx} - \frac{1}{A(x)} \mathcal{V} = 0 \tag{18}$$

where

$$A(x) = \int_0^1 \frac{\tilde{y}^2}{\mu(\phi(x,\tilde{y}))} d\tilde{y} \tag{19a}$$

$$B(x) = \int_0^1 \frac{\tilde{y}^2}{\mu(\phi(x,\tilde{y}))^2} \frac{\partial \mu(\phi(x,\tilde{y}))}{\partial x} d\tilde{y} \tag{19b}$$

Eqs. 15 and 16 give the axial and transverse velocities in terms of the volume fraction, ϕ, and hydrodynamic pressure, p. These may be substituted into the advection–diffusion equation, (10d), and, with the ODE for the hydrodynamic pressure equation, (18), they provide two coupled integro-differential equations for ϕ and p, which are difficult to solve numerically. However, in the next section, we are able to make further analytical progress by exploring the limit of a dilute suspension, $\phi \ll 1$.

Asymptotics for a Dilute Suspension

The coupled nonlinear system of Eq. 10 can be simplified by considering a dilute suspension of particles

$$\phi(x,y) = \epsilon \phi_1(x,y) \tag{20}$$

with $\epsilon \ll 1$ and ϕ_1 assumed to be $\mathcal{O}(1)$.

The osmotic pressure difference across the porous wall, in the dilute limit, is a linear function of the particle volume fraction at the wall[13]

$$\Delta\pi = \epsilon \pi_0 \phi_1(x, y=1) + \mathcal{O}(\epsilon^2) \tag{21}$$

where π_0 is a reference osmotic pressure related to the van't Hoff factor. In the dilute limit, the leading-order effect of volume fraction on viscosity is given by the Einstein viscosity[14]

$$\mu(\phi) = 1 + \frac{5}{2}\epsilon \phi_1 + \mathcal{O}(\epsilon^2) \tag{22}$$

Finally, the asymptotic expression for the effective diffusion coefficient, $D(\phi)$, for a dilute mono-disperse suspension is given by[15]

$$D(\phi) = 1 + \epsilon \chi \phi_1 \tag{23}$$

where the constant χ is a virial coefficient, a type-specific constant accounting for particle–particle interactions (see Elimelech et al.,[15] Batchelor[16] for tabulated values from the literature).

We exploit the dilute approximation by expanding the hydrodynamic pressure and velocity components as

$$p(x) = p_0(x) + \epsilon p_1(x) + \mathcal{O}(\epsilon^2) \tag{24a}$$

$$u(x,y) = u_0(x,y) + \epsilon u_1(x,y) + \mathcal{O}(\epsilon^2) \tag{24b}$$

$$v(x,y) = v_0(x,y) + \epsilon v_1(x,y) + \mathcal{O}(\epsilon^2) \tag{24c}$$

Substituting these expressions into the advection–diffusion equation for ϕ, Eq. 10d, the lowest-order terms are at $\mathcal{O}(\epsilon)$, and so this forms an equation for ϕ_1 in terms of the leading-order velocities u_0 and v_0

$$Pe\left(u_0 \frac{\partial \phi_1}{\partial x} + v_0 \frac{\partial \phi_1}{\partial y}\right) = \frac{\partial^2 \phi_1}{\partial y^2} \tag{25}$$

We note that the Brownian diffusivity, D_0, enters through the Péclet number and also that the concentration-dependent terms in the diffusivity only appear at order ϵ^2, and hence play no role. As a result, we need only consider a constant particle diffusivity, D_0, here. The symmetry and no-flux boundary conditions from (12a) and (12d) read

$$\frac{\partial \phi_1}{\partial y} = 0 \quad \text{on } y=0 \tag{26a}$$

$$Pe\mathcal{V}_0\phi_1 - \frac{\partial \phi_1}{\partial y} = 0 \quad \text{on } y=1 \tag{26b}$$

where $\mathcal{V}_0 = v_0(x,1)$ is the leading-order permeation flux at the porous channel walls. The inlet condition is

$$\phi_1(0,y) = \Phi_1(y) \tag{27}$$

for a normalized Gaussian function $\Phi(y)$ of the form given by Eq. 14.

The expression for the axial velocity given by (15) may be expanded in powers of ϵ, using the viscosity and pressure expansions (22) and (24a), to give

$$u(x,y) = \frac{dp_0}{dx}\frac{(y^2-1)}{2}$$
$$+ \epsilon\left(\frac{dp_1}{dx}\frac{(y^2-1)}{2} + \frac{dp_0}{dx}\int_y^1 \frac{5}{2}\tilde{y}\phi_1(x,\tilde{y})d\tilde{y}\right) + \mathcal{O}(\epsilon^2) \tag{28}$$

Similarly for the transverse velocity, given by (16), we find

$$v(x,y) = \frac{d^2p_0}{dx^2}\frac{(3y-y^3)}{6} + \epsilon\frac{\partial}{\partial x}\left\{\frac{dp_1}{dx}\frac{(3y-y^3)}{6}\right.$$
$$\left. -\frac{dp_0}{dx}\left[y\int_y^1 \frac{5}{2}\tilde{y}\phi_1(x,\tilde{y})d\tilde{y} + \int_0^y \frac{5}{2}\tilde{y}^2\phi_1(x,\tilde{y})d\tilde{y}\right]\right\} + \mathcal{O}(\epsilon^2) \tag{29}$$

Equations 28 and 29 determine the leading-order and order-ϵ components of the velocities u and v. As expected in the dilute limit, the presence of particles does not affect the leading-order problem; their effect is only felt at the next order.

The two cases for the boundary condition for v at $y=1$ (12b) take the form $\mathcal{V} = \mathcal{V}_0 + \epsilon\mathcal{V}_1$ where

$$\mathcal{V} = \mathcal{V}_0 + \epsilon\mathcal{V}_1$$
$$= \begin{cases} \mathcal{V}^* & \text{(Case 1)} \\ \kappa(p_0 - p_{\text{outer}}^0) + \epsilon\kappa[p_1 - p_{\text{outer}}^1 - \pi_0\phi_1(x,y=1)] & \text{(Case 2)} \end{cases} \tag{30}$$

Thus, there is no $\mathcal{O}(\epsilon)$ correction to the permeation flux for the case of constant outflow, that is, $\mathcal{V}_1 = 0$ in this case. However, for the pressure-dependent permeation flux, the leading-order outflow is proportional to the leading-order pressure difference across the membrane, and the $\mathcal{O}(\epsilon)$ outflow is related to the $\mathcal{O}(\epsilon)$ hydrodynamic pressure and the osmotic pressure.

Results

Leading-order velocities

Examining the $\mathcal{O}(1)$ velocity terms in the expansions (28) and (29), we find the leading-order velocity components $\boldsymbol{u}_0 = (u_0, v_0)$

$$u_0(x,y) = \frac{dp_0}{dx}\frac{(y^2-1)}{2} \tag{31a}$$

$$v_0(x,y) = \frac{d^2p_0}{dx^2}\frac{(3y-y^3)}{6} \tag{31b}$$

Note that the axial velocity, u_0, depends quadratically on the transverse coordinate, y, and the transverse velocity, v_0, depends cubically on y. Similar channel velocities may be found in the literature (e.g., see Probstein[2] for the case of a constant permeation flux). If the hydrodynamic pressure gradient, dp_0/dx, were constant, the leading-order velocities (31) would correspond precisely to Poiseuille flow. However, here we have the added interest that dp_0/dx may be a function of x. This means that, while the profile remains parabolic, its magnitude may vary due to the spatially varying hydrodynamic pressure, p_0. This variation must be determined case by case by considering the leading-order flow through the channel wall $\mathcal{V}_0$

$$v_0(x,1) = \mathcal{V}_0 = \frac{1}{3}\frac{d^2p_0}{dx^2} = \begin{cases} \mathcal{V}^* & \text{(Case 1)} \\ \kappa p_0 & \text{(Case 2)} \end{cases} \tag{32}$$

We note that, in solving for the leading-order hydrodynamic pressure p_0 from the ODE in (32), the constraints of constant flux at the channel inlet, (12e), and zero pressure at the outlet, (12f), are applied, which, for the leading-order problem, read as

$$\int_0^1 u_0 dy = 1, \quad \text{at } x=0 \tag{33a}$$

$$p_0 = 0, \quad \text{at } x=1 \tag{33b}$$

In the following, we consider each of these two cases, in turn.

Case 1: Constant Permeation Flux. In the case of constant flow through the porous walls, $\mathcal{V}_0 \equiv \mathcal{V}^* = \text{constant}$, the ODE for the leading-order hydrodynamic pressure, (32), with conditions (33) has solution

$$p_0 = 3(1-x)\left[1 - \frac{1}{2}\mathcal{V}^*(x+1)\right] \tag{34}$$

This function decreases with $\mathcal{V}^*$ for all x, that is, the greater the permeation flux the lower the required hydrodynamic pressure to maintain a constant flux. The leading-order flow then reads

$$\boldsymbol{u}_0 = (u_0, v_0) = \left(\frac{3}{2}(1-y^2) - \frac{3}{2}\mathcal{V}^*x(1-y^2), \frac{1}{2}\mathcal{V}^*(3y-y^3)\right) \tag{35}$$

from (31). The leading-order axial velocity $u_0 = u_0(x,y)$ and the transverse velocity $v_0 = v_0(y)$ are dependent on the magnitude of the flow through the walls. In the case of no permeation flux (impermeable walls), $\mathcal{V}^* = 0$, and (35) reduces simply to Poiseuille flow.

There is a maximum allowable constant permeation flux, $\mathcal{V}_{\text{max}}^*$, for which there is a positive net axial flow at the end of the channel; in this limiting case, all the fluid injected at the inlet passes through the porous walls. Exceeding this permeation flux results in back-flow from the channel outlet into the channel. The value of $\mathcal{V}_{\text{max}}^*$ is obtained by equating the influx of fluid with the flux through the channel walls, given by integrating the velocity v_0 (35) along the channel wall at $y=1$, resulting in a maximum permeation flux of $\mathcal{V}_{\text{max}}^* = 1$. As mentioned previously, another filtration process
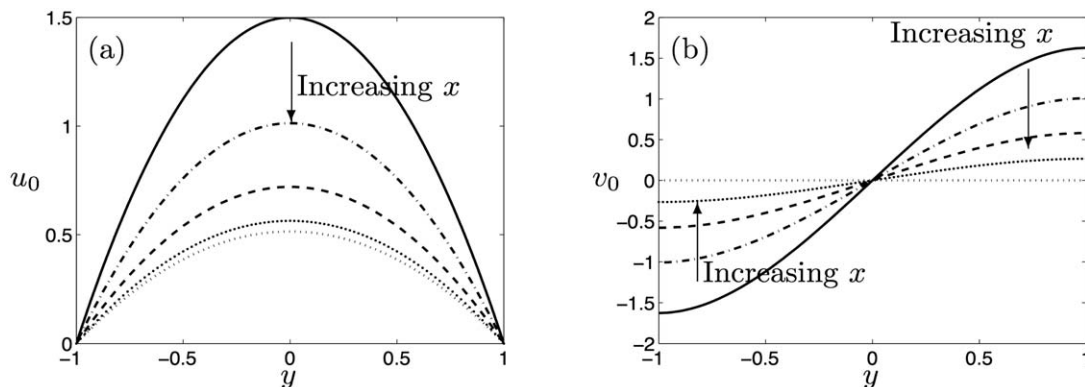
Figure 2. Profiles of the leading-order velocities for pressure-dependent permeation flux with $\kappa=1$ so that $\mathcal{V}_0=p_0$: (a) axial velocity, u_0 and (b) transverse velocity, v_0.

In each, the profiles are shown at $x=0$ (solid), $x=0.25$ (dot-dashed), $x=0.5$ (dashed), $x=0.75$ (dotted), and $x=1$ (skinny-dotted).

in which the flow is zero at the end of the channel (dead-end flow) is direct-flow filtration.[8]

Case 2: Pressure-Dependent Permeation Flux. We now determine leading-order solutions for the velocities, pressure, and volume fraction for a pressure-dependent permeation flux. For simplicity let us assume zero pressure outside the channel, $p_{\text{outer}} \equiv 0$. This corresponds to the common set-up in which the hydrodynamic outlet pressure and pressure outside the channel walls are equal. Later, this assumption is relaxed to explore the effect of a nonzero p_{outer}.

When the permeation flux through the wall is proportional to the hydrodynamic pressure, p, and osmotic pressure, π, then at leading order only the hydrodynamic pressure is significant, $\mathcal{V}_0=\kappa p_0$, as seen from Eq. 30. The leading-order transverse flow at $y=1$ (32) gives an ODE for the leading-order hydrodynamic pressure

$$\frac{1}{3}\frac{d^2p_0}{dx^2}=\kappa p_0 \qquad (36)$$

This ODE, subject to the boundary conditions (33), has solution

$$p_0=\sqrt{\frac{3}{\kappa}}\text{sech}\,\sqrt{3\kappa}\,\sinh\left[\sqrt{3\kappa}(1-x)\right] \qquad (37)$$

From this equation, we observe that the pressure, p_0, decreases with κ for all x and, as is the case for uniform permeation flux, the greater the permeation flux through the channel walls, the lower the required hydrodynamic pressure to achieve a constant influx. Substituting (37) into (31) determines the leading-order velocity field, (u_0, v_0). We note that, as $\kappa \to 0$ (in the limit of impermeable walls), $p_0 \to 3(1-x)$, and we recover Poiseuille flow, as expected. The components of the leading-order velocity field are shown in Figure 2 for $\kappa=1$. We observe that the leading-order axial velocity u_0 retains its parabolic profile along the channel though the amplitude decreases exponentially, because of the permeation of fluid through the channel walls. The leading-order transverse fluid velocity v_0, which has a cubic profile about $y=0$, also decreases in magnitude along the channel. This indicates the tendency of the fluid to move toward the porous walls of the channel but with an exponentially decaying rate along the channel.

### Numerical results for volume fraction

Having seen that the leading-order velocity fields and pressure gradient can be determined analytically in the two

cases of interest, we now turn our attention to determining the volume fraction profile, ϕ_1. Recall that the advection–diffusion equation, (25), with u_0 and v_0 given by our previous analysis, must be solved subject to the boundary conditions (26) and the Gaussian inlet particle distribution (27). We note that this initial condition does not satisfy the no-flux boundary condition (12d) and so there is a small transient over which this relaxes to a configuration that satisfies the boundary conditions. However, we choose to use this inlet condition as it provides a simple expression that elucidates the effect of a nonuniform particle volume fraction distribution, and we do not expect the behavior in the small transient to have an effect on the global system dynamics. This system is solved numerically, implementing a scheme in MATLAB (see Appendix A for details). As an illustrative example, Figure 3 depicts how an initial distribution in the channel develops downstream of the injection point, with $\sigma^2=0.05$, $Pe=3$, for the cases of: no permeation at the wall; constant permeation flux; and pressure-dependent permeation flux (with $\kappa=1$).

For the case of an impermeable wall, $\mathcal{V}^*=0$, we observe that the initial distribution spreads until it is essentially uniform across the width of the channel (Figure 3a). We note that, as the particles are initially localized in the center of the channel ($y=0$) where the transverse velocity is low as in Eq. 35, the transport of particles to the walls is slower than we would expect if the particles were injected with a uniform distribution. With permeation through the porous wall, particles still diffuse away from the center-line but now collect near the wall. This build-up of particles at the porous walls is known as concentration polarization.[1] In particular, for the case of constant permeation, the volume fraction of particles at the wall increases monotonically along the length of the channel (Figure 3b). When permeation is proportional to the pressure, the volume fraction at the walls is greatest about half way along the channel, as in Figure 3c. This is as a result of the transverse flow, which becomes smaller near the end of the channel after which point diffusion acts to move particles away from the wall.

Order-ϵ velocities

Having computed the leading-order velocity components, u_0 and v_0, and volume-fraction distribution ϕ_1, we are now in a position to compute the perturbation to the fluid flow caused by the presence of particles, that is, the $\mathcal{O}(\epsilon)$
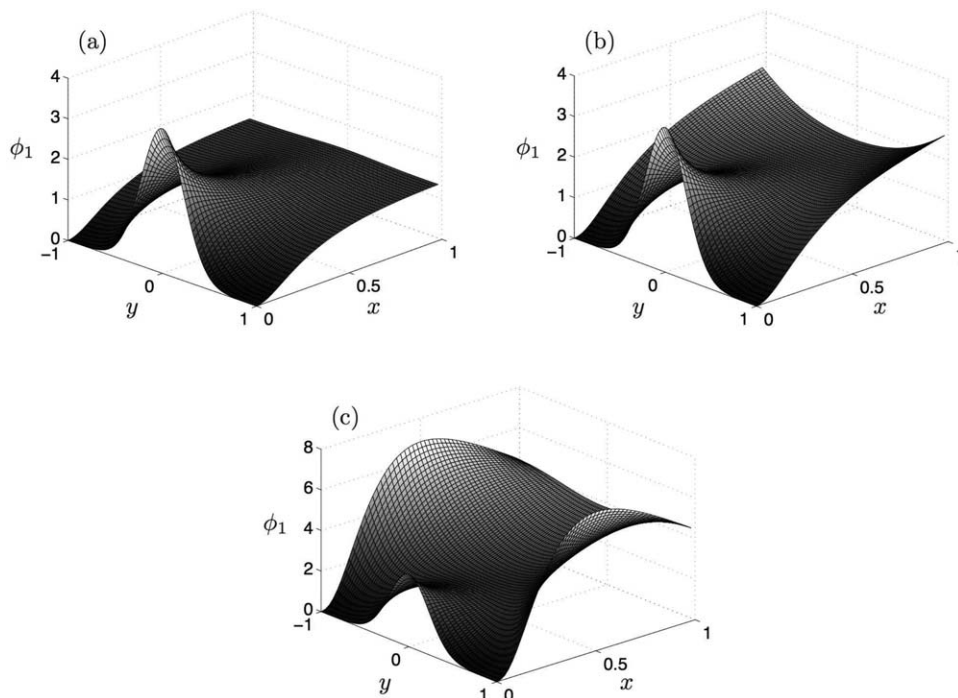
Figure 3. Profiles of the particle volume fraction ϕ_1 in the channel given by the solution to (25) with velocities (31).

(a) No permeation $\mathcal{V}^*=0$, ϕ_1 tends to a uniform state in the channel, (b) constant permeation $\mathcal{V}^*=0.25$, pressure given by (34), and (c) pressure-dependent permeation with p_0 given by (37). In (b) and (c) permeation flux results in particles collecting at the boundaries. In all computations, $Pe = 3$, $\sigma^2=0.05$, and for (c), $\kappa=1$.

corrections to the fluid velocity. From the axial and transverse velocities, (28) and (29), respectively, we have

$$u_1(x,y)=\frac{dp_1}{dx}\frac{(y^2-1)}{2}+\frac{dp_0}{dx}\int_y^1\frac{5}{2}\tilde{y}\phi_1(x,\tilde{y})d\tilde{y} \qquad (38a)$$

$$v_1(x,y)=\frac{\partial}{\partial x}\left\{\frac{dp_1}{dx}\frac{(3y-y^3)}{6}-\frac{dp_0}{dx}\left[y\int_y^1\frac{5}{2}\tilde{y}\phi_1(x,\tilde{y})d\tilde{y}\right.\right.$$
$$\left.\left.+\int_0^y\frac{5}{2}\tilde{y}^2\phi_1(x,\tilde{y})d\tilde{y}\right]\right\} \qquad (38b)$$

We note that a perturbation to the velocity, u_1, in principle affects the flux of fluid into the channel. However, the condition of constant fluid influx (12e), considering (33a), demands that

$$\int_0^1 u_1(0,y)dy=0 \qquad (39)$$

To ensure that this condition is satisfied, we must impose a perturbation to the hydrodynamic pressure at the inlet $x=0$, that is, $p_1(0)=\mathcal{P}\neq 0$. The value of $\mathcal{P}$ indicates how much harder we must push the liquid in the presence of particles to obtain the same fluid influx as would be obtained for a configuration in the absence of particles. The hydrodynamic pressure perturbation, p_1, may be found from the perturbed permeation flux $\mathcal{V}_1$ out of the channel wall at $y=1$

$$\frac{\partial}{\partial x}\left\{\frac{1}{3}\frac{dp_1}{dx}-\frac{dp_0}{dx}\int_0^1\frac{5}{2}\tilde{y}^2\phi_1(x,\tilde{y})d\tilde{y}\right\}=\mathcal{V}_1 \qquad (40)$$

using the transverse velocity (29). Here, $\mathcal{V}_1=0$ for the case of constant permeation flux through the channel walls and $\mathcal{V}_1=\kappa(p_1-\pi_0\phi_1)$ when the permeation flux is pressure-dependent, see Eq. 30. For each case, we may substitute for p_0 in Eq. 40 and solve subject to

$$p_1(0)=\mathcal{P}, \quad p_1(1)=0 \qquad (41)$$

and the flux condition (39) is applied to find $\mathcal{P}$.

By considering the initial volume fraction distribution given by (14), we may determine the dependence of $\mathcal{P}$ on the width of the distribution, σ. This gives us insight into the pressures required to transport a fixed flux of fluid containing a given distribution of particles through the channel for the two distinct cases of permeation flux through the channel walls, $\mathcal{V}_1$.

Case 1: Constant Permeation Flux. When there is constant flow through the boundary, $\mathcal{V}=\mathcal{V}^*$, and so, at order ϵ, $\mathcal{V}_1=0$. In this case, the ODE (40) to determine the order-ϵ pressure, p_1, becomes
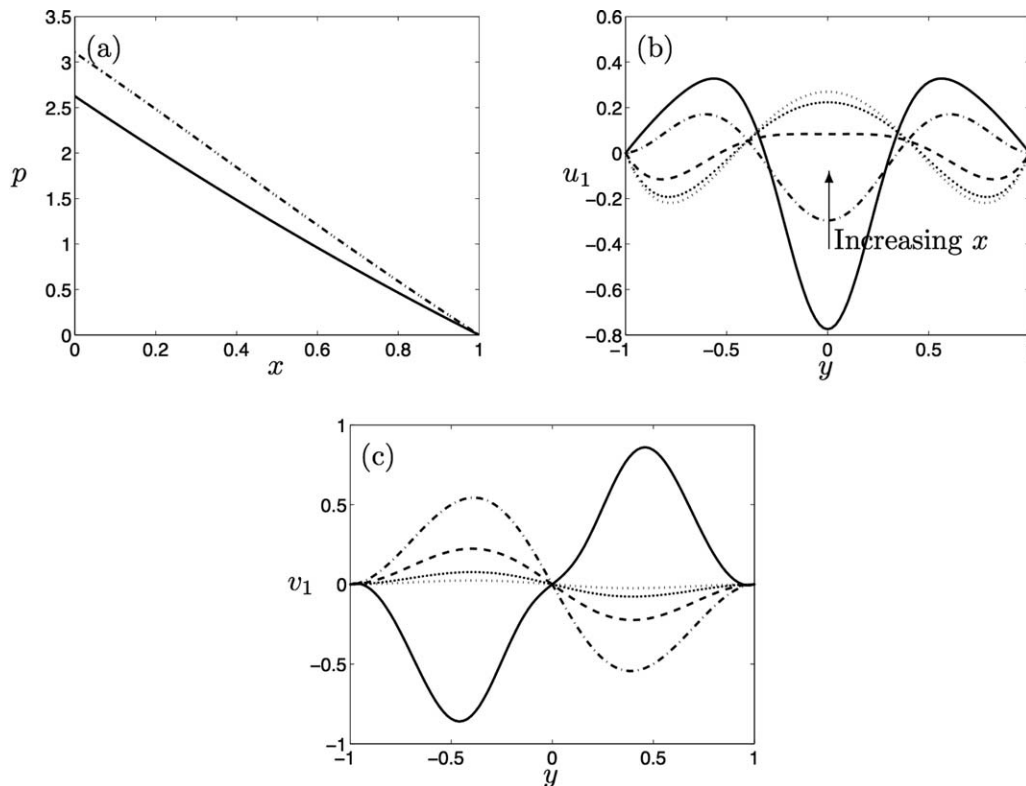
$$\frac{1}{3}\frac{d^2p_1}{dx^2}-\frac{\partial}{\partial x}\left\{\frac{dp_0}{dx}\int_0^1\frac{5}{2}\tilde{y}^2\phi_1(x,\tilde{y})d\tilde{y}\right\}=0 \qquad (42)$$

which has solution

$$p_1=\mathcal{P}(1-x)+3\int_0^x\left[\frac{dp_0(\tilde{x})}{d\tilde{x}}\int_0^1\frac{5}{2}\tilde{y}^2\phi_1(\tilde{x},\tilde{y})d\tilde{y}\right]d\tilde{x}$$
$$-3x\int_0^1\left[\frac{dp_0(\tilde{x})}{d\tilde{x}}\int_0^1\frac{5}{2}\tilde{y}^2\phi_1(\tilde{x},\tilde{y})d\tilde{y}\right]d\tilde{x} \qquad (43)$$

where we have applied the boundary conditions (41). Upon imposing the flux condition (39), the input pressure perturbation, $\mathcal{P}$, is related to the particle volume fraction through

$$\mathcal{P}=\frac{15}{2}\left\{\frac{dp_0(0)}{dx}\left(\int_0^1\tilde{y}^2\phi_1(0,\tilde{y})d\tilde{y}-\int_0^1\int_{\tilde{y}}^1 y'\phi_1(0,y')dy'd\tilde{y}\right)\right.$$
$$\left.-\int_0^1\left[\frac{dp_0(\tilde{x})}{d\tilde{x}}\int_0^1\tilde{y}^2\phi_1(\tilde{x},\tilde{y})d\tilde{y}\right]d\tilde{x}\right\} \qquad (44)$$

Figure 4. Pressure and order-ϵ velocity profiles given by (38) for the case of constant permeation flux through the channel walls, $\mathcal{V}^* = 0.25$.

(a) The hydrodynamic pressure, $p = p_0 + \epsilon p_1$, for $\epsilon = 0.05$ (dot-dashed) is plotted with the leading-order term, p_0 (solid), (b) Profile of the order-ϵ axial velocity perturbation, u_1, for $x=0$ (solid), $x=0.25$ (dot-dashed), $x=0.5$ (dashed), $x=0.75$ (dotted), and $x=1$ (skinny-dotted), and (c) profile of order-ϵ transverse velocity perturbation, v_1, for $x=0$ (solid), $x=0.25$ (dot-dashed), $x=0.5$ (dashed), $x=0.75$ (dotted), and $x=1$ (skinny-dotted). In the computations, $Pe = 3$, $\sigma^2 = 0.05$.

We note that this relationship is nonlocal, depending on the behavior of the particles along the entire length of the channel. Substituting for $\mathcal{P}$ into (43) provides the pressure perturbation, p_1, and, along with ϕ_1, allows us to calculate the perturbations to the velocity field u_1 and v_1 using the order-ϵ velocities (38).

In Figure 4a, we illustrate the pressure for the profile ϕ_1 with $\sigma^2 = 0.05$ and $Pe = 3$, as shown in Figure 3b. As expected, the pressure perturbation is positive for all x: the hydrodynamic pressure in the channel required to maintain the same fluid influx as the case in which no particles are present is increased as a result of the increase in viscosity. The perturbation to the axial velocity, u_1, is shown in Figure 4b. Recall that the leading-order axial velocity here is a Poiseuille profile, decreasing in magnitude as we move down the channel. We see that, in regions of high particle volume fraction, u_1 is negative and so the total axial velocity, u, is decreased by the presence of particles, whereas in regions of lower particle volume fraction u_1 is positive and so the total axial velocity is increased. By conservation of mass, (10a), a perturbation in the axial velocity results in a perturbation in the transverse velocity, v. As there is an accumulation of particles near the walls, that is, the region of high volume fraction moves to the walls, the location of the position of maximum retardation in the transverse direction caused by the perturbation to the flow moves toward the walls as we move down the channel (Figure 4b). Hence, while the perturbed transverse velocity, v_1 (38b), initially increases, as

there is no perturbed permeation through the walls, that is, $v_1(x, 1) = 0$, the fluid must ultimately be transported back toward the center of the channel; this is signified by a change in sign of v_1 further along the channel, as seen in Figure 4c.

The relationship between the pressure perturbation at the inlet, $\mathcal{P}$, and the width of the particle distribution, σ, for various constant permeation fluxes, $\mathcal{V}^*$, is shown in Figure 5. Because the addition of particles increases the viscosity of the fluid, and the hydrodynamic pressure gradient is related to the viscosity through the momentum equation, (10b), we expect that a greater hydrodynamic pressure will be required to maintain a constant influx. However, we find that there is a critical value of σ that maximizes the additional pressure, $\mathcal{P}$. This means, surprisingly, that there is an inlet particle distribution width that requires the largest additional (perturbed) pressure, whereas the pressure perturbation increases as the permeation flux increases (Figure 6a). The pessimal value of the distribution width, σ_{pess}, decreases linearly with permeation flux, $\mathcal{V}^*$ (Figure 6b). The values of σ around this pessimal pressure perturbation reflect inlet distributions that have significant volume fraction gradients across the channel. Hence, the viscosity has a significant gradient in the channel, globally, and thus the particles have a greater effect on the resulting flow. It is found that both "thinner" and "fatter" volume fraction distributions require less additional pressure to maintain a constant fluid influx: for larger values of σ, the volume fraction distribution is more uniform and so
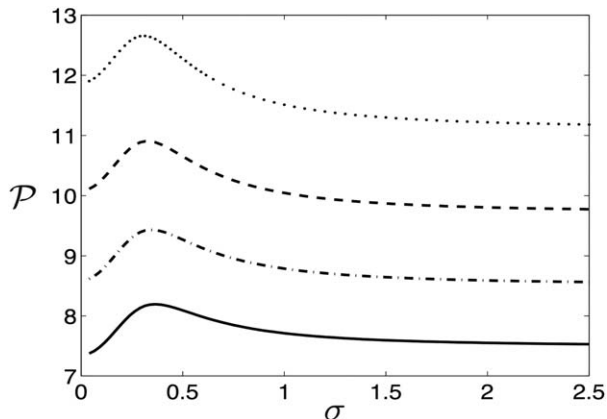
Figure 5. Variation of the pressure perturbation parameter $\mathcal{P}$ given by (44) with σ for the case of constant permeation flux: $\mathcal{V}^*=0$ (solid), $\mathcal{V}^*=0.2$ (dot-dashed), $\mathcal{V}^*=0.4$ (dashed), and $\mathcal{V}^*=0.6$ (dotted).

As σ increases, $\mathcal{P}$ tends to a constant, with a nontrivial behavior showing a critical value of σ that maximizes $\mathcal{P}$. Note that $\mathcal{P} \to 15/2$ as $\sigma \to \infty$ when $\mathcal{V}^*=0$. In the computations, $Pe = 3$.

there is less variation to the flow due to the concentration-dependent viscosity, whereas for smaller values of σ the volume fraction is largely confined to a small region that does not significantly affect the viscosity for large regions of the channel.

In the case of no flow through the porous walls (impermeable walls, $\mathcal{V}^*=0$) there is an analytic asymptote for $\mathcal{P}$ as $\sigma \to \infty$, namely $\mathcal{P} \to 15/2$ (see Figure 5, solid line). This may be calculated using the expression for p_0 from (34) and the equation for $\mathcal{P}$ (44), as in the limit $\sigma \to \infty$, $\phi \equiv 1$. However, in the case of porous walls, concentration polarization along the channel walls results in ϕ_1 no longer being spatially independent in the channel. This precludes the analytical calculation of the asymptote that is observed numerically in the limit $\sigma \to \infty$, see Figure 6a. The asymptotic value of $\mathcal{P}$ increases with the magnitude of the permeation flux.

Although the leading-order hydrodynamic pressure, p_0, required to maintain a constant influx decreases with increasing

permeation flux, it is observed in Figure 5 that the $\mathcal{O}(\epsilon)$ hydrodynamic pressure, p_1, increases with increasing permeation flux. This arises as a result of there being no $\mathcal{O}(\epsilon)$ permeation flux in this case. Particles aggregate at the walls because of the leading-order permeation flux; by increasing the permeation flux, $\mathcal{V}^*$, this increases the accumulation of particles at the wall, and thus the local viscosity, so more pressure is required to advect these particles along the channel.

Case 2: Pressure-Dependent Permeation Flux. When there is a pressure-dependent flow through the porous channel walls, the $\mathcal{O}(\epsilon)$ permeation flux through the walls is given by $\mathcal{V}_1=\kappa[p_1-\pi_0\phi_1(x,y=1)]$. The ODE for the hydrodynamic pressure, (40), then becomes

$$\frac{d^2p_1}{dx^2}-3\kappa p_1=3g(x) \tag{45}$$

with boundary conditions (41), where

$$g(x) := \frac{\partial}{\partial x}\left\{\frac{dp_0}{dx}\int_0^1 \frac{5}{2}\tilde{y}^2\phi_1(x,\tilde{y})d\tilde{y}\right\}-\kappa\pi_0\phi_1(x,1) \tag{46}$$

The homogeneous adjoint problem to (45) only permits the trivial zero solution; the Fredholm Alternative Theorem[17] then implies that the ODE in (45) with boundary conditions (41) has a unique solution. This solution can be found using the method of variation of parameters, giving

$$\begin{aligned}
p_1=\mathcal{P}\cosh\left(\sqrt{3\kappa}x\right)+3\int_0^x \Bigg[&\cosh\left(\sqrt{3\kappa}[x-\tilde{x}]\right)\frac{dp_0(\tilde{x})}{d\tilde{x}} \\
&\times\int_0^1 \frac{5}{2}\tilde{y}^2\phi_1(\tilde{x},\tilde{y})d\tilde{y}\Bigg]d\tilde{x} \\
+\sqrt{\frac{3}{\kappa}}\frac{dp_0(0)}{dx}&\sinh\left(\sqrt{3\kappa}x\right)\Bigg(\int_0^1\int_{\tilde{y}}^1 \frac{5}{2}y'\phi_1(0,y')dy'd\tilde{y} \\
&-\int_0^1 \frac{5}{2}\tilde{y}^2\phi_1(0,\tilde{y})d\tilde{y}\Bigg) \\
-\sqrt{3\kappa}\pi_0&\int_0^x \phi_1(\tilde{x},1)\sinh\left(\sqrt{3\kappa}[x-\tilde{x}]\right)d\tilde{x}
\end{aligned} \tag{47}$$

where we have imposed the boundary condition (41a) and flux condition (39). Imposing the final boundary condition (41b), we determine the relationship between the additional pressure, $\mathcal{P}$, and the particle distribution ϕ_1
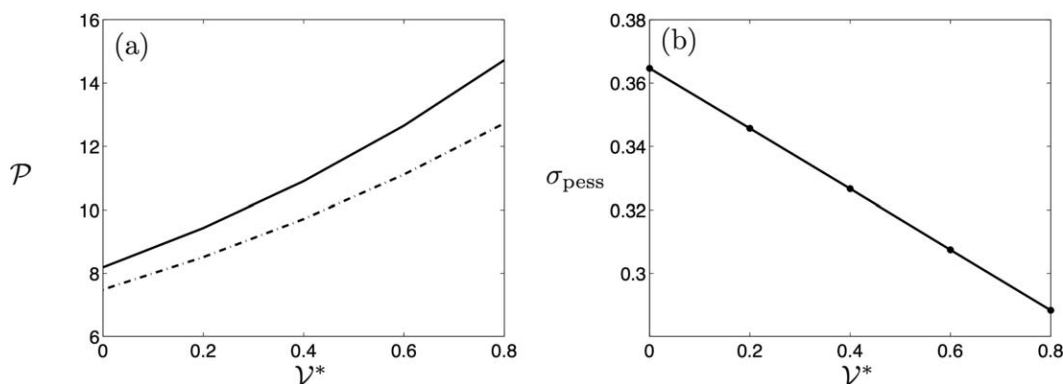
Figure 6. (a) The pessimal pressure perturbation, $\mathcal{P}_{\text{pess}}$ (solid), and the asymptotic pressure perturbation, $\mathcal{P}_{\text{asym}}$ (dot-dashed), as $\sigma \to \infty$, for the case of a constant permeation flux $\mathcal{V}=\mathcal{V}^*$, and (b) the distribution width resulting in the pessimal pressure, σ_{pess}.

In the computations, $Pe = 3$.
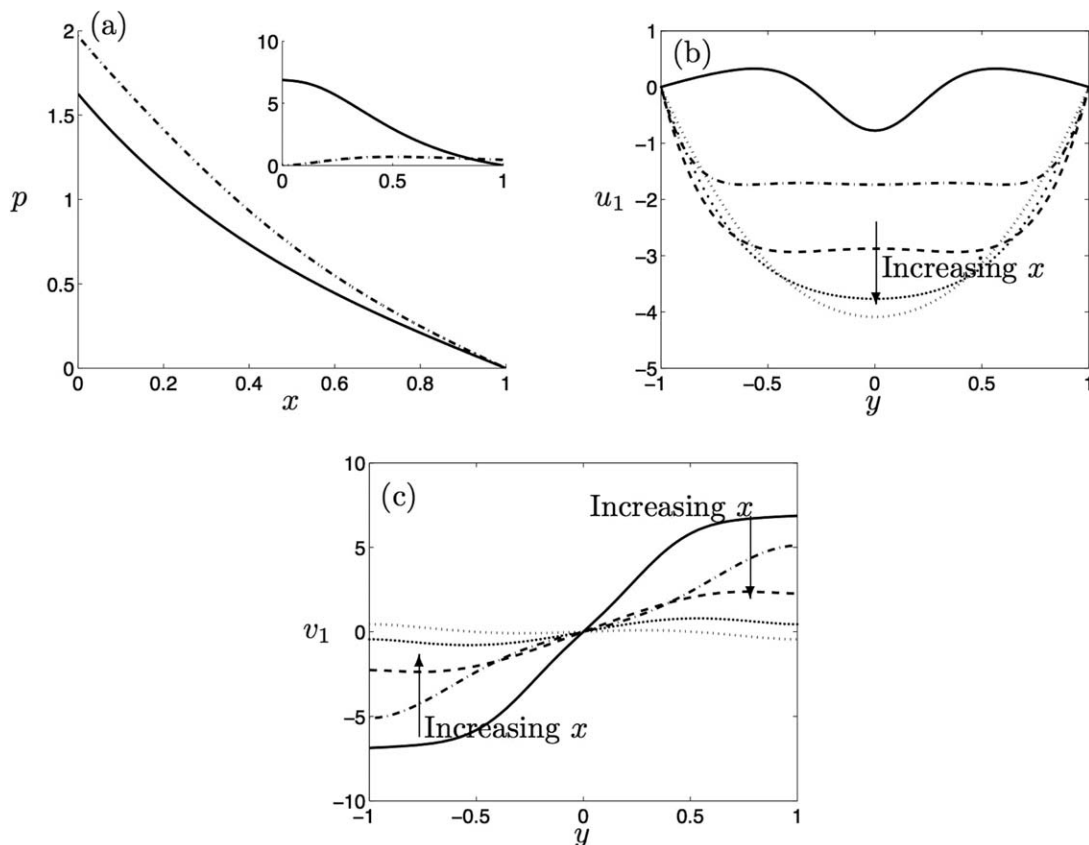
Figure 7. Pressure and order-ϵ velocity profiles given by (38) for the case of pressure-dependent permeation flux through the channel walls, $\mathcal{V}_1 = \kappa[p_1 - \pi_0 \phi_1(x, 1)]$.

(a) The hydrodynamic pressure, $p = p_0 + \epsilon p_1$ for $\epsilon = 0.05$ (dot-dashed) is plotted with the leading-order term, p_0 (solid). The inset shows the pressure perturbation, p_1 (solid), and the osmotic pressure (dot-dashed) in the channel. (b) Profile of order-ϵ axial velocity perturbation, u_1, at $x=0$ (solid), $x=0.25$ (dot-dashed), $x=0.5$ (dashed), $x=0.75$ (dotted), and $x=1$ (skinny-dotted), and (c) profile of order-ϵ transverse velocity perturbation, v_1, at $x=0$ (solid), $x=0.25$ (dot-dashed), $x=0.5$ (dashed), $x=0.75$ (dotted), and $x=1$ (skinny-dotted). In the computations, $Pe = 3$, $\sigma^2 = 0.05$, and $\pi_0 = 0.1$.

$$\mathcal{P} = \sqrt{\frac{3}{\kappa}} \tanh\sqrt{3\kappa}\, \frac{dp_0(0)}{dx}$$

$$\times \left(\int_0^1 \frac{5}{2}\tilde{y}^2 \phi_1(0, \tilde{y}) d\tilde{y} - \int_0^1 \int_{\tilde{y}}^1 \frac{5}{2} y' \phi_1(0, y') dy' d\tilde{y} \right)$$

$$- 3\,\text{sech}\sqrt{3\kappa} \int_0^1 \left[\cosh\left(\sqrt{3\kappa}[1-\tilde{x}]\right) \frac{dp_0(\tilde{x})}{d\tilde{x}} \int_0^1 \frac{5}{2}\tilde{y}^2 \phi_1(\tilde{x}, \tilde{y}) d\tilde{y} \right] d\tilde{x}$$

$$+ \sqrt{3\kappa}\pi_0 \text{sech}\sqrt{3\kappa} \int_0^1 \phi_1(\tilde{x}, 1) \sinh\left(\sqrt{3\kappa}[1-\tilde{x}]\right) d\tilde{x}$$

$$\tag{48}$$

Given ϕ_1, we may solve (48) for $\mathcal{P}$ and then the pressure p_1 and the $\mathcal{O}(\epsilon)$ velocities u_1 and v_1 follow immediately from (47) and (38).

We illustrate the resulting behavior by considering the injection of particles with distribution width $\sigma = \sqrt{0.05}$, so that ϕ_1 is as shown in Figure 3c. The reference osmotic pressure is taken to be $\pi_0 = 0.1$ here. We note that, while the quantitative results are affected by changes in π_0, the qualitative features are unaffected and as such we choose to hold the parameter constant in the results presented here. The behavior of p_0 and p_1 and the osmotic pressure are then as shown in Figure 7a. We observe that the hydrodynamic pressure perturbation, p_1, is positive corresponding to an increase in the total hydrodynamic pressure in the channel. However,

there is an axial position beyond which the osmotic pressure, $\Delta\pi$, exceeds the hydrodynamic pressure perturbation. This is unavoidable as $p_1 = 0$ at $x = 1$, and this has an impact on the permeation flux observed.

The flow perturbation u_1 is shown in Figure 7b. Near the entrance to the channel, u_1 is negative in the center of the channel, where there is a high volume fraction so the total axial flow is lower than the leading-order (particle-free) flow; in regions of low particle volume fraction, u_1 is positive and so the total axial flow is greater than in the absence of particles, similar to the case of constant permeation flux. However, further down the channel u_1 is negative across the entire channel. This is due to the order-ϵ transverse permeation flux, which causes fluid to be removed from the channel. In this case, the perturbation to the transverse velocity, v_1, (see Figure 7c) increases the total transverse velocity toward the walls over the entire length of the channel. This induces an additional fluid flux through the channel walls which also advects particles toward the walls, increasing the osmotic pressure due to concentration polarization up to the point where it exceeds the hydrodynamic pressure (see Figure 7a). This excess osmotic pressure results in a net inward flow (classic osmosis), which is undesirable in filtration because it reduces the amount of pure water that is produced by filtration. Hence, near the end of the channel this osmotic inflow is unavoidable, when $p_{\text{outer}} = 0$. However, as the particles in the channel do not affect the leading-order flow,
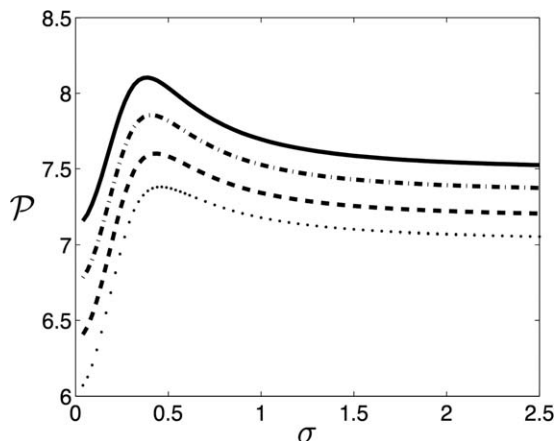
Figure 8. Variation of the pressure perturbation parameter, $\mathcal{P}$, given by (48) with σ for the case of pressure-dependent permeation flux through the channel walls, $\mathcal{V}_1 = \kappa[p_1 - \pi_0 \phi_1(x, 1)]$ with $\kappa = 0.25$ (solid), $\kappa = 0.5$ (dot-dashed), $\kappa = 0.75$ (dashed), and $\kappa = 1$ (dotted).

As σ increases $\mathcal{P}$ tends to a constant, again with a nontrivial behavior showing a critical σ at which $\mathcal{P}$ is maximized. In the computations, $Pe = 3$ and $\pi_0 = 0.1$.

there is no osmotic inflow of fluid at leading order, and the outflow through the channel walls tends to zero at the end of the channel (as $p=0$ at $x=1$).

The relationship between $\mathcal{P}$ and σ is shown in Figure 8 for different constants of proportionality, κ, for the pressure-dependent permeation flux. A similar functional relationship to Case 1 for constant permeation flux is observed, specifically the existence of a pessimal distribution of particles. As for Case 1, when $\mathcal{V}^* \neq 0$ there is no simple analytical asymptote as $\sigma \to \infty$. The value of the distribution width resulting in the pessimal pressure perturbation increases linearly with κ (Figure 9a), however, the pessimal pressure perturbation is observed to decrease with κ, in an approximately linear fashion (provided κ exceeds a certain value, $\kappa \approx 0.3$) as in Figure 9b. Similarly to Case 1, the leading-order hydrodynamic pressure in the channel, (37), is reduced by the permeation flux. However, this case differs in that the asymptote for $\mathcal{P}$ as $\sigma \to \infty$ decreases as the permeation flux through the channel walls increases through an increase in wall permeability in κ. This decrease is approxi-

mately linear for $\kappa \gtrsim 0.3$, as in Figure 9b. Hence, less pressure is required to ensure a constant influx of fluid for higher wall permeabilities when particles are present in the channel. This result is a consequence of the osmotic component of $\mathcal{P}$, which becomes increasingly negative with κ and so causes the reduction in the pressure perturbation. This suggests that the component of the channel for which there is a net fluid outflow and which acts as an effective filter is shorter because more fluid is lost through the walls earlier in the channel, reducing the hydrodynamic pressure, p, required to maintain a given fluid influx.

Total permeate

A quantity of particular interest is the total flux of fluid that flows out through the porous walls, F. This is given by the integral of the transverse velocity along the wall

$$F = 2 \int_0^1 v(x, 1) dx$$

$$= 2 \int_0^1 (v_0(x, 1) + \epsilon v_1(x, 1)) dx = F_0 + \epsilon F_1 \quad (49)$$

(Here, the factor of two is due to the symmetry of the system about $y=0$.) This is easily calculated for the constant permeation-flux case as here $\mathcal{V} = \mathcal{V}^*$ for all $0 \leq x \leq 1$, and so the total fluid flux passing through the porous walls is simply $F = 2\mathcal{V}^*$.

For the pressure-dependent permeation flux case, the leading-order total flux may also be calculated analytically as $F_0 = 2(1 - \mathrm{sech}\sqrt{3\kappa})$, an increasing function of κ as would be expected. However, the order-ϵ term must be calculated numerically. The interesting feature of the order-ϵ term, F_1, is that it is dependent on the particles in the flow. In addition, there is an osmotic inflow of fluid toward the end of the channel that reduces the net permeate flux. Consequently, both the inlet distribution width, σ, and the Péclet number, Pe, influence the result (Figure 10a). For lower Péclet numbers, more localized distributions (lower values of σ) result in larger fluxes, but for larger Péclet numbers, more spatially uniform distributions (larger values of σ) produce larger fluxes. Analyzing the pressure perturbation parameter, $\mathcal{P}$, with Péclet number (Figure 10b), we see that, as the Péclet number is increased, a greater pressure is required to maintain a constant influx. As an increase in Péclet number also increases the permeation flux, this suggests a direct
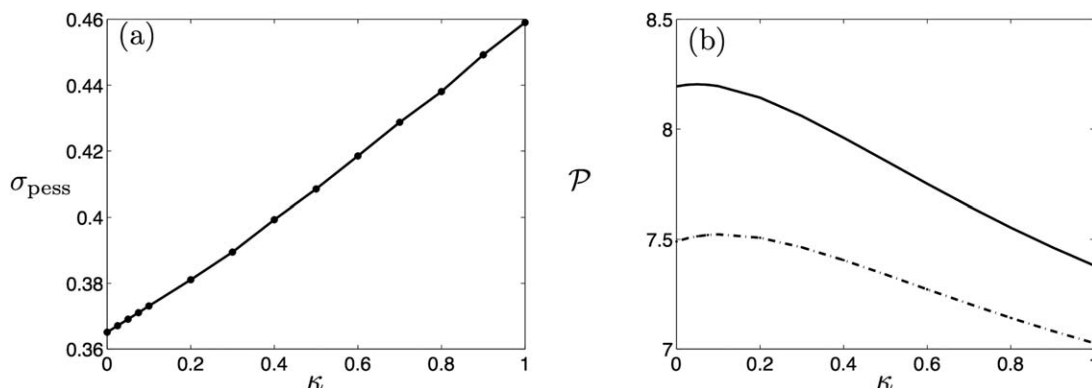
Figure 9. (a) The distribution width resulting the pessimal pressure, σ_{pess} and (b) the pessimal pressure perturbation, $\mathcal{P}_{\mathrm{pess}}$ (solid), and the asymptotic pressure perturbation, $\mathcal{P}_{\mathrm{asym}}$ (dot-dashed), as $\sigma \to \infty$, for different channel wall permeabilities, κ.
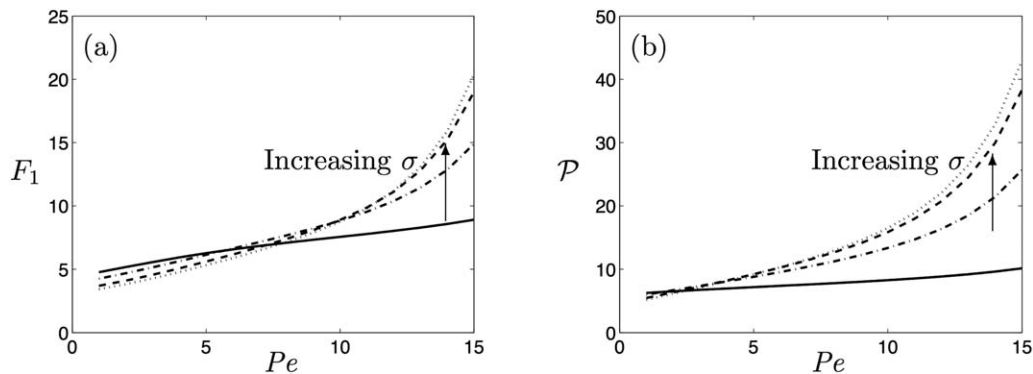
In the computations, $Pe = 3$ and $\pi_0 = 0.1$.

Figure 10. (a) Order-ϵ flux through the channel walls as a function of Péclet number, *Pe*, for σ=0.2 (solid), σ=0.4 (dot-dashed), σ=0.75 (dashed), and σ=1.5 (skinny-dotted).

(b) Pressure perturbation parameter, $\mathcal{P}$, against Péclet number for σ=0.2 (solid), σ=0.4 (dot-dashed), σ=0.75 (dashed), and σ=1.5 (skinny-dotted). In the computations, *Pe*=3 and π_0=0.1.

correspondence between hydrodynamic pressure and permeation flux, as one would expect.

Pressure Outside the Channel

In the previous section, we concluded that it is an inevitable consequence of the osmotic pressure that an $\mathcal{O}(\epsilon)$ flux of fluid enters the channel through its walls in a pressure-dependent permeation flux. In water filtration, this effect, at any order, is undesirable. Here, we consider a modified set-up that eliminates this inflow by setting the pressure outside the channel, p_{outer}, to be a nonzero constant. The effective total transmembrane pressure may then be written as

$$\Delta p - \Delta \pi = p_0(x) - p_{\text{outer}} + \epsilon[p_1(x) - \pi_0 \phi_1(x,1)] \quad (50)$$

We retain, without loss of generality, the condition that the fluid pressure, p, is zero at the end of the channel. By choosing p_{outer} appropriately, we can ensure that the effective total transmembrane pressure remains nonnegative over the entire length of the channel.

Osmotic pressure is again negligible in the leading-order problem and the leading-order permeation flux is given here by $\mathcal{V}_0 = \kappa(p_0 - p_{\text{outer}})$ (cf. Eq. 30). The leading-order transverse flow at $y=1$ (32) gives an ODE for the leading-order pressure

$$\frac{1}{3}\frac{d^2 p_0}{dx^2} = \kappa(p_0 - p_{\text{outer}}) \quad (51)$$

which on application of boundary conditions (33) yields

$$p_0(x) = p_{\text{outer}}\left[1 - \text{sech}\,\sqrt{3\kappa}\cosh\left(\sqrt{3\kappa}x\right)\right]$$
$$+ \sqrt{\frac{3}{\kappa}}\text{sech}\,\sqrt{3\kappa}\sinh\left(\sqrt{3\kappa}[1-x]\right) \quad (52)$$

The leading-order velocities (u_0, v_0) may be calculated by substituting (52) into Eq. 19b. These, in turn, may be used to calculate the volume fraction of particles, ϕ_1, in the channel by solving the advection–diffusion equation, (10d).

If $p_{\text{outer}} > 0$ then the pressure difference across the membrane, and thus the permeation flux, is reduced which in turn increases the hydrodynamic pressure, (52), required to maintain a constant influx. As the permeation flux is reduced, concentration polarization at the channel walls is reduced. However, as $p=0$ at $x=1$, there is a point in the channel at which $p < p_{\text{outer}}$ and so there is an induced leading-order permeation influx from the outside into the channel through the channel walls. This inflow does not occur at leading order with $p_{\text{outer}}=0$. Hence, a positive outer pressure decreases particle collection at the wall but results in an influx. Conversely, if $p_{\text{outer}} < 0$ then the pressure difference across the membrane is increased, increasing the
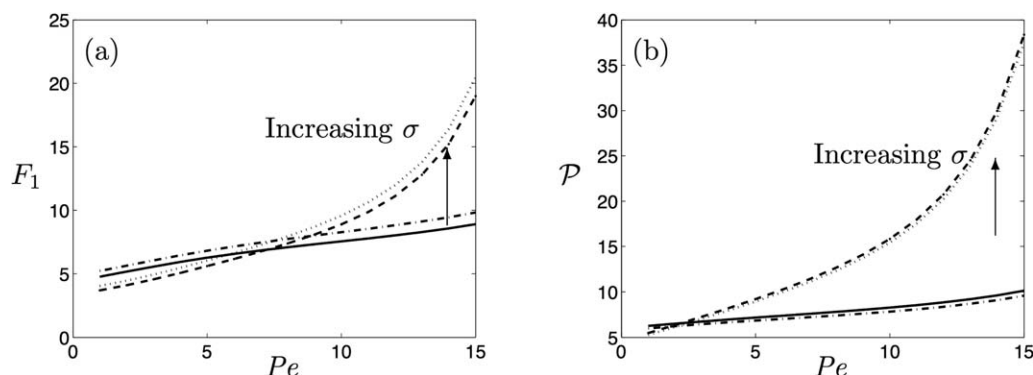
Figure 11. (a) Order-ϵ flux through the channel walls as a function of Péclet number, *Pe*, for σ=0.2 with zero outer pressure (solid) and an order-ϵ outer pressure $p_{\text{outer}} = -\pi_0\phi_1(1,1)$ (dot-dashed), and σ=0.75 (dashed, skinny-dotted, respectively).

We see that the order-ϵ outer pressure increases the fluid flux. (b) Pressure perturbation parameter, $\mathcal{P}$, as a function of Péclet number for σ=0.2 with zero outer pressure (solid) and an order-ϵ outer pressure $p_{\text{outer}} = -\pi_0\phi_1(1,1)$ (dot-dashed), and σ=0.75 (dashed, skinny-dotted, respectively). We see that the order-ϵ outer pressure decreases the pressure perturbation parameter. In the computations, *Pe*=3 and π_0=0.1.

permeation flux which in turn decreases the required hydrodynamic pressure, (52). Here, we do not have an influx of fluid into the channel at any position at leading order if p_{outer} is larger in magnitude than the osmotic pressure (order-ϵ). However, as the permeation flux is increased, there is a greater concentration polarization effect at the channel walls. Hence, a negative outer pressure ensures a number of outcomes. First, no fluid leaks into the channel from the walls. From a water-filtration perspective this means that none of the filtered water re-enters the channel. Second, we increase the permeation flux at the walls resulting in more fluid being filtered. The penalty in doing so is the extra energy required to generate the negative external pressure and also the increase in particle collection at the walls.

The leading-order total permeate, F_0, for a nonzero p_{outer}, reads

$$F_0 = 2\left(1 - \text{sech}\,\sqrt{3\kappa}\right) - 2\sqrt{\frac{\kappa}{3}}p_{\text{outer}}\tanh\sqrt{3\kappa} \qquad (53)$$

using (49). We note that F_0 is a decreasing function of p_{outer} for all κ, and the critical point ($F_0 = 0$) beyond which there is a net influx occurs when $p_{\text{outer}} = \sqrt{3/\kappa}\,\tanh\sqrt{3\kappa}/2$. Furthermore, the order-ϵ total permeate, F_1, is a decreasing function of the outside pressure for all Pe and σ.

Order-ϵ outer pressure

We wish to choose the outer pressure to avoid any re-entry of fluid into the channel through the walls. In the previous section, we saw that this might be achieved using a sufficiently large negative outer pressure. However, we also want to reduce the energy required to generate this additional pressure, so it is the "optimum" outer pressure that is of interest. As re-entry is an order-ϵ effect due to the osmotic pressure, we assume that p_{outer} is $\mathcal{O}(\epsilon)$. Now the leading-order pressure is given by Eq. 37 and F_0 does not depend on p_{outer} and remains as in the case of $p_{\text{outer}} = 0$, that is, $F_0 = 2\left(1 - \text{sech}\,\sqrt{3\kappa}\right)$. Also, as F_0 differs between the cases of an outer pressure and no outer pressure, a better comparison of how the particles affect the flow is to consider an outer pressure that is of order-ϵ.

As the leading-order problem remains unchanged, and the re-entry is a result of the osmotic pressure exceeding the hydrodynamic pressure near the exit of the channel, we take p_{outer} to be equal and opposite to the osmotic pressure at the exit of the channel, that is

$$p_{\text{outer}} = -\epsilon\pi_0\phi_1(1,1) \qquad (54)$$

The transmembrane pressure difference now reads

$$\Delta p - \Delta\pi = p_0(x) + \epsilon\{p_1(x) - \pi_0[\phi_1(x,1) + \phi_1(1,1)]\} \qquad (55)$$

This leads to a modification to the $\mathcal{O}(\epsilon)$ pressure given by Eq. 47 and the pressure perturbation given by Eq. 48. In this case the terms $\phi_1(\tilde{x},1)$ in the final term of each equation are replaced with $\phi_1(\tilde{x},1) - \phi_1(1,1)$.

The choice of outer pressure that negates the osmotic effect does indeed prevent any influx of fluid from outside the channel through the walls, with transverse velocity giving a permeation flux out of the channel at each point along the wall. This results in a greater $\mathcal{O}(\epsilon)$ permeate flux F_1 as seen in Figure 11a as well as a reduction in the pressure perturbation $\mathcal{P}$ as in Figure 11b.

By choosing p_{outer}, (54), in this way, we ensure that no fluid leaks into the channel from the walls. However, in terms of the energy penalty in doing so, the analysis here provides a mechanism for determining the minimum suction pressure required to ensure that no filtered fluid re-enters the channel, thus optimizing the filtration operation if the actual outlet gauge is zero ($p = 0$ at $x = 0$). For a positive outlet pressure, p_{outer} could be zero or even positive.

Conclusions

The flow and particle distribution for a dilute suspension in a channel flow with porous walls has been described. The presence of particles reduces the flow velocity by increasing the viscosity of the fluid. Allowing permeation (either constant or pressure dependent) through the porous walls reduces the pressure required for the fluid to flow at a constant influx. This permeation flux also contributes to the transport of particles from the center of the channel to the channel walls, leading to concentration polarization when the walls are impermeable to particles.

We considered the effect of varying the width of an inlet pulse of particles in the cross-stream channel direction. Beginning with a very narrow pulse (relatively highly concentrated in a small region around the center of the channel), we observe that, as this pulse width increases, it initially becomes harder to push the particles and fluid at the same rate, that is, a higher inlet hydrodynamic pressure is required. This is attributed to the size of the region of the channel occupied by the particles: for small widths the particles do not affect a significant region of the channel to alter the fluid flow; however, as this pulse width increases, the particles affect a greater proportion of the fluid and so a greater pressure is required to transport the particles with a constant fluid influx. Interestingly, however, this increase in pressure reverses as the width of the inlet distribution of particles surpasses a critical value and it becomes easier (less pressure is required) to transport the particles. We attribute this observation to the lower gradients of particle volume fraction in the channel, as the particles are now more uniformly distributed. Thus overall we observe a critical pessimal value of the inlet distribution width that maximizes the additional pressure required.

In the case of pressure-dependent permeation flux, concentration polarization results in the osmotic pressure exceeding the hydrodynamic pressure at the end of the channel which leads to an inward flow from the porous channel walls. In a filtration system, this situation of pure fluid entering the channel contaminated by particles is undesirable yet unavoidable due to the condition of equal outlet pressure and pressure outside the channel.

Finally, we analyzed the effect of a constant outer pressure to the channel walls in an effort to eliminate the occurrence of clean water re-entry. A positive outer pressure decreases concentration polarization at the channel walls but again there is an unavoidable influx of fluid through the channel walls. A negative outside pressure increases the permeation flux, with no influx, but at the cost of increased concentration polarization and energy expenditure. Applying an outer pressure that is equal and opposite to the osmotic pressure at the end of the channel negates the influx caused by osmosis. As the magnitude of the outer pressure is small, it is a reasonable compromise in terms of additional energy required to prevent the re-entry of fluid into the channel.

The results presented here provide new observations into a model problem related to water filtration that may offer insight into operating strategies.

Acknowledgment

Notation

x = axial direction
y = transverse direction
u = axial velocity
v = transverse velocity
p = hydrodynamic pressure
D = diffusion coefficient
a = particle radius
Q = inlet flow rate
Pe = Péclet number
Re = Reynolds number
F = total permeate
$\mathcal{V}$ = permeation velocity
$\mathcal{V}^*$ = constant permeation velocity
$\mathcal{P}$ = pressure perturbation at $x=0$
H = typical channel height
L = typical channel length
U = typical channel velocity

Greek letters

μ = viscosity
ϕ = particle volume fraction
π = osmotic pressure
π_0 = reference osmotic pressure
κ = permeability
δ = channel aspect ratio
σ = standard deviation of particle distribution
ϵ = small parameter
χ = virial coefficient

Subscripts

outer = outside the channel
0 = leading-order
1 = order-ϵ

Literature Cited

1. Song L, Elimelech M. Theory of concentration polarization in cross-flow filtration. *J Chem Soc Faraday Trans*. 1995;91:3389–3398.
2. Probstein RF. *Physicochemical Hydrodynamics: An Introduction*. Butterworths, 1989.
3. Kostoglou M, Karabelas AJ. Mathematical analysis of fluid flow and mass transfer in a cross flow tubular membrane. *Ind Eng Chem Res*. 2009;48:5885–5893.
4. Davis RH, Sherwood JD. A similarity solution for steady-state cross-flow microfiltration. *Chem Eng Sci*. 1990;45:3203–3209.
5. Davis RH, Leighton DT. Shear-induced transport of a particle layer along a porous wall. *Chem Eng Sci*. 1987;42:275–281.
6. Bowen WR, Williams PM. Prediction of the rate of cross-flow ultrafiltration of colloids with concentration-dependent diffusion coefficient and viscosity—theory and experiment. *Chem Eng Sci*. 2001;56:3083–3099.
7. Bacchin P, Si-Hassen D, Starov V, Clifton MJ, Aimar P. A unifying model for concentration polarization, gel-layer formation and particle deposition in cross-flow membrane filtration of colloidal suspensions. *Chem Eng Sci*. 2002;57:77–91.
8. Pearce GK. *UF/MF Membrane Water Treatment: Principles and Design*. Water Treatment Academy, 2011.
9. Leighton D, Acrivos A. The shear-induced migration of particles in concentrated suspensions. *J Fluid Mech*. 1987;181:415–439.
10. Sandblom (Alfa-Laval) RM. Filtering Process. *Swedish Patent* 7,416,257, 1978.
11. Beavers GS, Joseph DD. Boundary conditions at a naturally permeable wall. *J Fluid Mech*. 1967;30:197–207.
12. Shipley RJ, Waters SL, Ellis MJ. Definition and validation of operating equations for poly(vinyl alcohol)-poly(lactide-co-glycolide) microfiltration membrane-scaffold bioreactors. *Biotechnol Bioeng*. 2010;107:382–392.
13. Williams FA. A nonlinear diffusion problem relevant to desalination by reverse osmosis. *SIAM J Appl Math*. 1969;17:59–73.
14. Guazzelli É, Morris JF. *A Physical Introduction to Suspension Dynamics*. Cambridge University Press, 2012.
15. Elimelech M, Gregory J, Jia X, Williams RA. *Particle Deposition and Aggregation. Measurement, Modelling and Simulation*. Butterworth-Heinemann, 1995.
16. Batchelor GK. Brownian diffusion of particles with hydrodynamic interaction. *J Fluid Mech*. 1976;74:1–29.
17. Keener JP. *Principles of Applied Mathematics*. Westview, 2000.
18. Morton KW, Mayers DF. *Numerical Solution of Partial Differential Equations*. Cambridge University Press, 2005.

Appendix A: Numerical Scheme

We exploit symmetry about the y axis to consider the domain $(x, y) \in [0, 1] \times [0, 1]$, and discretize this domain by introducing grid points

$$x_i = hi, \quad i = 0, 1 \ldots N \tag{A1a}$$

$$y_j = kj, \quad j = 0, 1 \ldots M \tag{A1b}$$

for grid spacings h and k where $h = \Delta x = 1/N$ and $k = \Delta y = 1/(M-1)$. We index the variable ϕ as follows

$$\phi_{i,j} = \phi_1(x_i, y_j) \tag{A2}$$

The resulting solutions are then mapped to the other half of the domain, $-1 \leq y < 0$. A forward-center finite difference scheme for the advection–diffusion equation, (25), is

$$\phi_{i+1,j} = \phi_{i,j}$$
$$+ \frac{2h}{p'(x_i)(y_j^2 - 1)} \left(-p''(x_i) \frac{3y_j - y_j^3}{6} \frac{\phi_{i,j+1} - \phi_{i,j-1}}{2k} \right.$$
$$\left. + \frac{1}{Pe} \frac{\phi_{i,j+1} - 2\phi_{i,j} + \phi_{i,j-1}}{k^2} \right) \tag{A3a}$$

$$\phi_{i+1,1} = \phi_{i,1} - \frac{2h}{p'(x_i)} \left(\frac{2}{Pe} \frac{\phi_{i,2} - \phi_{i,1}}{k^2} \right) \tag{A3b}$$

$$\phi_{i+1,M} = \frac{2\phi_{i+1,M-1} - \frac{1}{2}\phi_{i+1,M-2}}{\frac{3}{2} - kPe v_{i+1,M}} \tag{A3c}$$

$$\phi_{1,j} = \Phi(y_j) \tag{A3d}$$

for $i = 1, 2, \ldots N-1$ and $j = 2, 3, \ldots M-1$. The standard forward-center finite difference discretization for nonboundary points of the advection–diffusion equation, (25), is given in (A3a), with the symmetry condition $\partial \phi_1 / \partial y = 0$ at $y = 0$ given by (A3b) and the no-flux boundary condition given by (A3c). There is an initial condition of some $\phi(0, x) = \Phi$ (A3d). The scheme (A3) is second-order accurate.

For a constant-coefficient convection–diffusion equation

$$f_x + a f_y = b f_{yy} \tag{A4}$$

with $b > 0$, there are two mesh size parameters to consider

$$v = \frac{a \Delta x}{\Delta y}, \quad \eta = b \frac{\Delta x}{\Delta y^2} \tag{A5a,b}$$

Implementing a stable forward in x, central-differences in y finite-differences scheme, it is required that[18]

$$0 < v \leq 1, \quad 0 < \eta \leq \frac{1}{2} \tag{A6}$$

In our governing equations, the advection–diffusion Eq. 10d for the volume fraction ϕ_1 does not have constant coefficients, but the coefficients are well behaved, with no singularities. We ensure that the scheme is stable by requiring $\Delta x / \Delta y^2 = 1/50 \ll 1/2$ for stability: we use $\Delta y = 2 \times 10^{-2}$ and $\Delta x = 8 \times 10^{-6}$.